5
Results

We have made a systematic study on the synthesis of boron doped carbon nanotubes in a high vacuum chemical vapour deposition system. After each deposition, a SEM image showed the existence of nanotubes and could guide us in which temperature the tubes were preferentially grown. TEM images and a detailed Raman analysis could provide us with the information that SWNTs were being synthesized, and a comparison with the spectra of a pure carbon SWNT sample gave an evidence that the tubes were doped with boron.

At last, a XPS analysis together with theoretical calculations, provided us with the final evidence for the doping and allowed to make a doping quantification among the samples.

The used experimental set up, catalyst, precursors, every growth parameters, characterizations and results will be explained on the next sections.

5.1
Experimental set up

This section regards a concern about the dimensions of the quartz tube used on the HVCVD scheme, and can be thought as a growth parameter. This concern is based on the fact that we found that boron compounds are probably being deposited on the quartz tube, and for a given section of the quartz tube, the ratio V_{olume}/S_{urface} grows with the diameter and is $R/2$, where R is the inner radius of the quartz tube. This mean that for a large diameter tube, there will be less boron deposited on the wall in comparison to the boron atoms there are flowing to the sample, and in this case, a greater amount of boron will reach the SWNTs. And for a greater length into the furnace's hot zone, a greater amount of boron will be deposited into the tube's wall, thus for a larger hot zone, a less amount of boron atoms will reach the sample.

In this way, it is important to say that the crucible was located in the middle of the hot zone, and the length of this zone is $\sim$22.4cm for our furnace, and the inner diameter of the quartz tube is $\sim$2.74cm. It is also important to say that we could not test the hypothesis of the influence of those dimensions on the growth of the samples. But we believe that different geometries can be

Table 5.1: Growing conditions

Precursor	Vapour pressure used (torr)	Growing time (min)
Ethanol	65	10
Triisopropyl borate	7	10
Triethyl borate	13	10

the explanation of observed discrepancies between the experiments found on the literature, such as the observed shift of the G band described on the last chapter. Just to maintain the coherence along the text, we will explain those discrepancies on the next chapter, after the presentation of our results.

5.2 Catalyst and precursors

As a catalyst, we have used a powder that consisted of a mixture of Magnesium Oxide and Iron(III) nitrate in a 2:1 mass proportion (31). Both powders were sonicated in a Isopropyl alcohol solution for 24 hours and then stirred in a hot plate around 70^0C until the formation of a uniform mixture of a dry orange powder. The hole process usually took 4 days to be completed. The function of the Iron(III) nitrate is to provide iron particles as catalyst to the growth of the SWNTs while the function of the porous Magnesium Oxide powder is to prevent the agglomeration of those iron particles into clusters, preventing the formation of SWNTs (31). The catalyst was reduced insitu at 700^0C by passing a flow of H_2 at 65torr during 10min before the nanotube growth.

Three different precursors were used in this work. In order to have a reference carbon SWNT sample to be compared with the other samples, 65torr of the vapour pressure of Ethanol (Sigma Aldrich $\geq$ 99.5%) were used during a 10min growth at different temperatures.

Triisopropyl borate $C_9H_{21}BO_3$ (Fluka $\geq$ 97%) was used as carbon and boron precursor in order to reproduce the boron doped single wall nanotube that was obtained in other experiments (33, 32). The samples produced by this feedstock were compared with the samples prepared by Triethyl borate $C_6H_{15}BO_3$ (Sigma Aldrich 99%), which is the precursor that we have dedicated a longer fraction of this study. It is important to notice that Triethyl borate was never used before on the synthesis of boron doped carbon nanotubes. The main reason to choose those two feedstocks is because they have carbon and boron atoms on the same molecular structure, that is a great advantage to the HVCVD system. Table 5.1 lists the parameters used for those precursors.

The reasons for the use of so different vapour pressures is due to the

different intrinsic vapour pressure of those precursors. And the reason for the chosen values, is to maximize the amount of molecules reaching the catalyst for each substance.

We are basically going to focus on Triethyl borate on the next sections, since this study is essentially about the use of this precursor and the produced tubes.

5.3 SEM images

After each growth, the sample was carried to a JEOL JSM 6701F field emission scanning electron microscope. The obtained images shows that almost no tubes were formed above 900^0C and bellow 740^0C for the samples prepared using Triethyl borate. For this reason, we studied the temperature range starting at 740^0C and increasing it by 20^0C until 900^0C.

It is possible to identify between the images, that the tubes are preferentially formed around 800^0C. It is clear that Triethyl borate produces a greater amount of tubes than Ethanol. The SEM images of the sample prepared by Triethyl borate are shown in Fig 5.1.

It is possible to observe the presence of catalysts on Fig 5.1. However, one question that can arise, is of which material are those empty spaces on the samples prepared at 740^0C and 900^0C made? The answer will come on the XPS section, when we point out that those samples have a lower amount of carbon and a bit higher amount of magnesium when compared, for example, with the sample prepared at 800^0C. This leads to the conclusion that those volumes without tubes are not made of some carbon allotrope such as amorphous carbon.

For comparison, Fig 5.2 shows a sample prepared using Ethanol as a precursor. By analysing several images, it is clear that Ethanol produces less tubes than Triethyl borate for the same temperature synthesis.

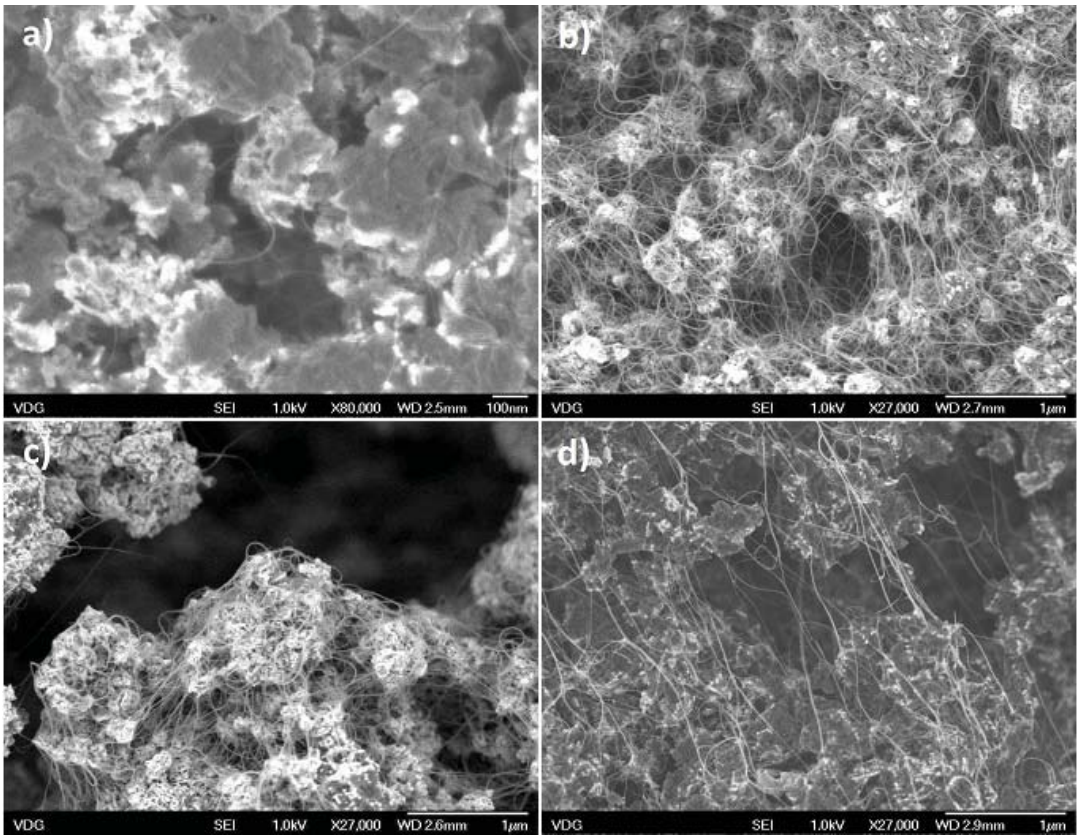

Figure 5.1: Typical SEM images of tubes produced using Triethyl borate at a) 740^0C, b) 800^0C, c) 840^0C, and d) 900^0C.

Figure 5.2: SEM images of a reference sample produced using Ethanol at 850^0C. This temperature gives the highest amount of produced tubes for this precursor.

We also have an image of a sample produced by Triethyl borate at 800^0C, performed by a JEOL JEM-2100 transmission electron microscopy operated at

200KV. Despite the high electron energy that damages the tubes, it is possible to confirm the presence of SWNTs with diameter around 1nm. This image is shown at Fig 5.3.

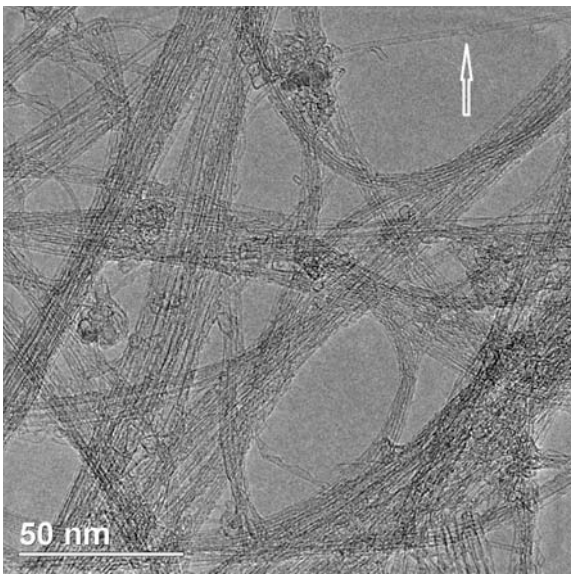

Figure 5.3: TEM image of a sample prepared using Triethyl borate at 800^0C. It is possible to confirm the presence of SWNTs with diameter around 1nm.

The use of a SEM as an analysing tool provided us with fundamental knowledge about the amount of tubes produced at each temperature and among the tested precursors. It is possible to conclude by those images, that both boron containing feedstocks produce a larger amount of tubes in comparison to Ethanol. However, no tested temperature used for the synthesis using Triisopropyl borate produced a comparable amount of tubes when compared to the growth of tubes using Triethyl borate at 800^0C.

It is difficult to have any conclusion about the length of the tubes among different precursors. It is possible to observe that the bundles have a length that is at least on the μm scale, and some images shows that these values can be greater than 10μm for some bundles produced with the boron containing precursor. However, in order to investigate the length dependence, we would have to grow tubes at different time intervals for each precursor.

As will be described on the next section, Raman analysis was performed in each sample after the microscopy section.

5.4 Raman

The basic concept of Raman spectroscopy of a molecule is that a photon with energy E_i is absorbed by an electron on the ground and on the vibrational

state i, thus making the electron go to an excited state. Then it goes back to the ground electronic state and to a final vibrational state f that is different from i while emits a photon with energy E_f. This measured shift $E_i - E_f$ is what allows the structural information of the molecule to be obtained from the Raman measurement. This process is different for the crystalline structure where the excited electron creates a phonon that has a momentum. Since part of the energy goes to the created phonon via a electron-phonon interaction, the emitted photon will reveal some properties of the solid (11).

This kind of spectroscopy takes advantage of the high Raman cross section for sp^2 carbon structures in the visible range, and then, is a powerful technique used to characterize carbon nanotubes, since it can determine if the tubes are single, double or multi wall, provides chirality information, defect information on the structure, among other several issues (44, 3, 11, 45, 46, 47). All required information about this technique will be explained on the next sections.

Raman has contributed a lot for this work, since it can probe changes on the Fermi level of the nanotube (48, 40). As described on preceding chapter, boron doping lowers the Fermi level of the SWNTs, thus Raman technique can provide an evidence for doping in the case of the spectra show a shift of this energy level (48, 40).

After the SEM characterization, every sample was taken to a confocal NT-MDT NTegra spectrometer equipped with a 473nm laser. We performed several measurements at different points of each sample. We took care to repeat the same laser intensity conditions for all samples, since a different laser power would lead to erroneous results, as will be explained later. The measured power of the laser hitting the sample was around 0.125mW. This value will be justified next on the text. Since the area of the spot was nearly the same for every measurement, the laser intensity was almost the same for every spectra.

At last, I must say the we performed Raman measurements on the reduced catalyst and found no peaks at any region of interest.

5.4.1
Raman spectra: The Radial Breathing mode (RBM)

The Radial Breathing Mode, or RBM, is a peak around 100cm^{-1} to 350cm^{-1} that is related to the radial vibration of the tube, and the position of this peak can be related to its diameter (45, 44, 47). This peak rises with higher intensity when the photon excites an electron between the Van Hove singularities in what is called resonant Raman (45). Since the energy distance E_{ii} of the those singularities are bigger for the decreasing diameter, each tube

will have a enhanced RBM peak for a laser energy around E_{ii}. The plot that relates the diameter of the tubes and laser energy is called Kataura Plot (49) and is shown in Fig 5.4.

It is important to note that our laser energy is 2.62eV, so it important to keep in mind that the diameters measured for our tubes are not necessary all the diameters presented on the sample.

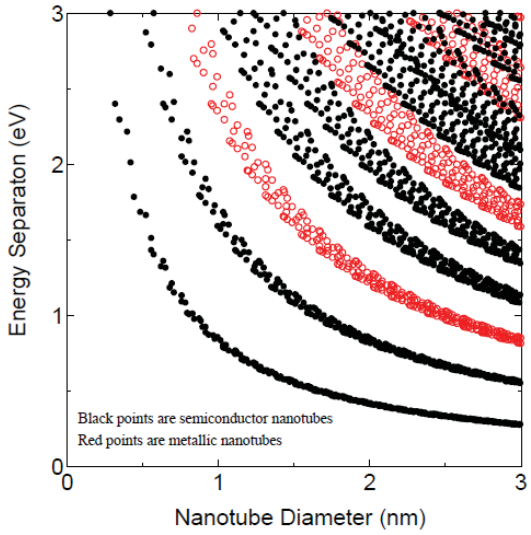

Figure 5.4: Katura plot from Dr. Prof. Shigeo Maruyama's page (http://www.photon.t.u-tokyo.ac.jp/ maruyama/index.html).

The RBM peaks of the tubes produced with Ethanol are shown in Fig 5.5. This figure shows three different production temperatures. It shows that we are producing SWNTs and allows us to calculate the diameters of the interacting tubes on the resonant Raman process. It is possible to observe diameters ranging from 1.0nm to 1.3nm, that according to the Fig 5.4, corresponds to semiconducting tubes. It is also possible to observe, that despite the position of the peaks does not change with the production temperature, it is clear that the relative intensity changes among them and that the diameters distribution becomes wider with the increasing temperature, for our laser line.

Diameters ranging from 0.8nm to 1.3nm can be observed on the samples produced by Triethyl borate, showing no dependence of the diameter with the used precursor. It is important to note that similar to the Ethanol case, tubes with same diameters are being produced among different temperatures but with a different relative intensity among the RBM peaks, and there is a tendency to produce large diameter tubes at higher temperatures, as reported for other production methods of pure carbon nantubes (3). It is important to notice that those peaks are in accordance with the TEM image described

above. The RBM peaks of the tubes obtained for this precursor can be found in Fig 5.6.

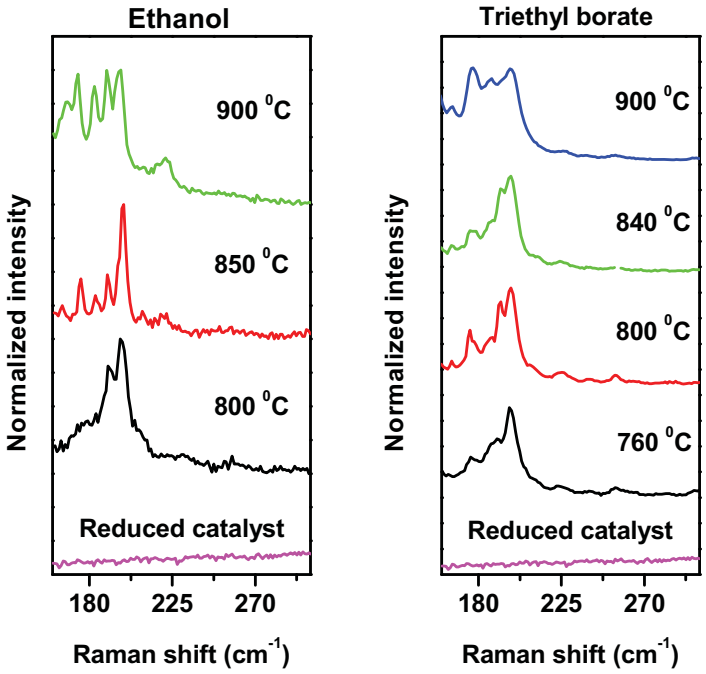

Figure 5.5: On the left, RBM of samples prepared with Ethanol at different temperatures and the Raman spectra of the reduced catalyst at the same region

Figure 5.6: On the right, RBM of samples prepared with Triethyl borate at different temperatures and the Raman spectra of the reduced catalyst at the same region.

Of course we are assuming that the tubes have a low doping content, since we have made the calculation of the diameter as if the tubes were a pure carbon SWNTs. As explained on the preceding chapter, the density of states and thus the Van Hove singularities are expected to have a low modification for the low boron content on the tubes. Such assumption will be justified on the next section, where we will show the behaviour of the D band among the samples.

5.4.2 Raman spectra: The D band

The D band peak is located around 1350cm^{-1}, for the 2.62eV laser, and can be observed in all sp^2 carbon based material. This is a disorder induced band and supply us with informations about the disorder concentration on

the structure. One of the useful information that the D band can provide is a qualitative disorder evaluation among the samples through the I_D/I_G relation, where I_D is the intensity of the D band while I_G is the intensity of the G band, that is a allowed Raman band that will be described on the next section (44).

Fig 5.7 shows the D band spectra of the samples produced by Triethyl borate. Just for comparison, the G band around 1500-1600cm^{-1} is also shown in this figure.

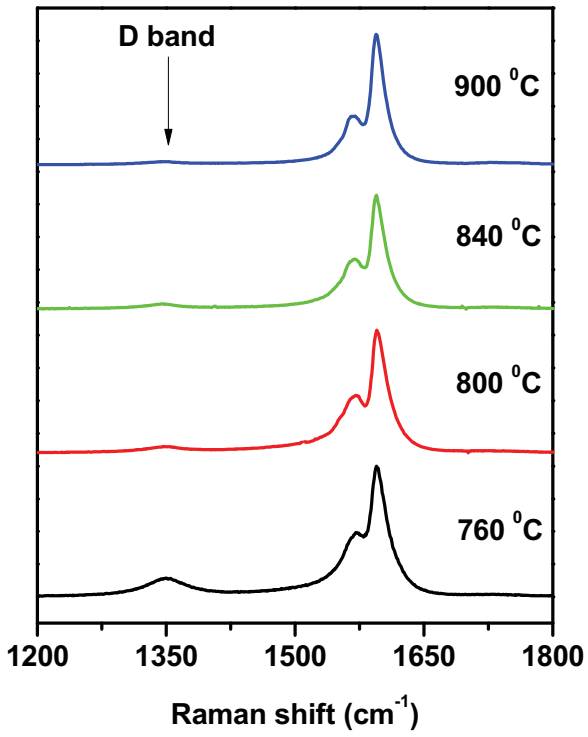

Figure 5.7: Plot of D and G bands of the Raman spectra of the tubes produced by Triethyl borate. The arrow indicates the position of the D band.

Tubes synthesized using Ethanol have a larger I_D/I_G relation when compared to the tubes prepared by the both boron containing precursor. It indicates that ethanol may not be a good precursor for carbon nanotubes. As shown in Fig 5.7 or 5.8, the intensity of this band decreases with the increasing growing temperature. Since the boron doping on the carbon SWNT acts as if it were a defect, the low intensity for this band observed on the boron containing samples may suggests a low doping level. It is important to remember that similar situation was observed for low boron doped tubes prepared by laser ablation (36).

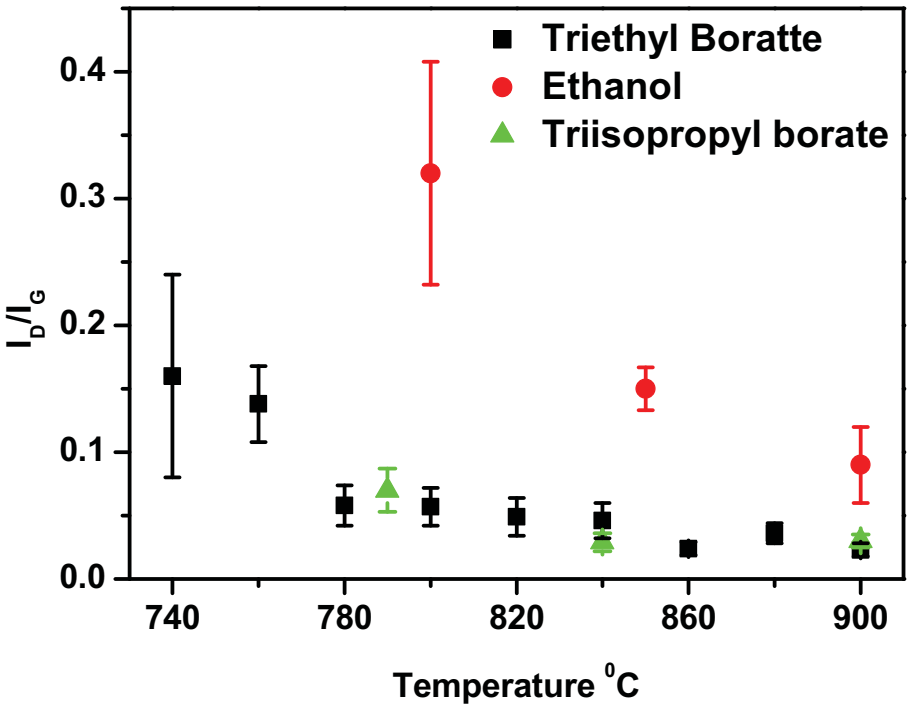

Figure 5.8: I_D/I_G for both boron containing samples and the reference samples. The error bars are due to different points on the sample.

The decreasing D band intensity with the increasing temperature does not mean that the doping level is also decreasing. That is because other factors, such as different production temperatures can change de formation and so the quality of the tubes, as can be observed on Fig 5.8 for the reference samples.

Regarding the doping, the D band analysis only provides information that if the tubes are doped, then the doping content is low. But it does not provide any evidence for that. Despite of this, the only true information about the use of Thiethyl borate as a precursor, is that as well as Triisopropyl borate, it synthesizes higher quality tubes regarding the defects on the structure. But there is an important question about this result: Is the boron on the precursor or the boron on the tubes that are lowering this band or maybe Ethanol is just not able to provide high quality tubes? Our guess is that those two effects of boron on the precursor or on the tubes may contribute together to lower the D band. As pointed on the preceding chapter, the substitutional method to dope the tubes after their synthesis improves the graphitization of MWNTs (41), however, the higher intensity of this band for the reference sample can also be explained by the fact that ethanol may not be a good precursor.

5.4.3
Raman spectra: The G band

The G band is a first order allowed Raman active band presented in all sp^2 carbon materials (44, 3, 11). This band, for carbon nanotubes, can be understood by the zone folding method of graphene, (3) described on the last section of the second chapter, and is related to the in plane stretching of the C-C bonds (11). This band is located around 1580cm^{-1} in graphene, however, due to the cylindrical structure of SWNTs that causes a permanent strain along the circumferential direction, six bands appears on chiral nanotubes and three on achiral tubes, but usually, only two bands related to the A_1 symmetry mode dominate the spectrum (11). The higher frequency of the A_1 mode is called G^+ band while the lower frequency is called G^- band and their positions are at 1591cm^{-1} and 1565cm^{-1} on SWNTs respectively (11).

The G band spectra for our samples is characteristic of SWNTs with evident splitting into the G^- and G^+ bands for all precursors used and is well fitted by four Lorentzians, two of them corresponding to unresolved A_1 and E_1 symmetry modes and the other two corresponding to the E_2 symmetry mode at 1550cm^{-1} and 1606cm^{-1}. Fig 5.9 shows typical G bands for our samples prepared with Triethyl borate at different temperatures.

This band is sensitive to several features of the tubes, including the diameter that can be probed by the G^- band (44, 11), the metallic character of the tubes, provided that the correct laser energy is being used (46) and the direction of the SWNTs bundles that can be probed through polarized Raman measurements (50). However, the most useful feature that we found for this work is the possibility of probing changes on the Fermi level of the tubes by looking for a shift on this band position (40, 48, 51).

Since this band position is also sensitive to the temperature (52, 11), and in order to avoid a misinterpretation of the results, we took care to use the same laser power during the same amounts of time for all samples. In order to select a laser power that did not disturb our results, we measured the G^+ band position for the reference sample and for a boron containing sample at different laser power. As expected, Fig 5.10 shows a softening on this band position for a high laser power (11). It is also possible to observe that for a power below $\sim$0.13mW, this band position remains constant for both samples, and at $\sim$1591cm^{-1} for the reference sample, that is the value predicted for carbon SWNTs (44, 11). This plot justifies the use of $\sim$0.13mW power for all the Raman measurements on this Thesis.

It is also possible to observe on Fig 5.11, that the position of this peak is upshifted in comparison to the reference sample produced by Ethanol. We also

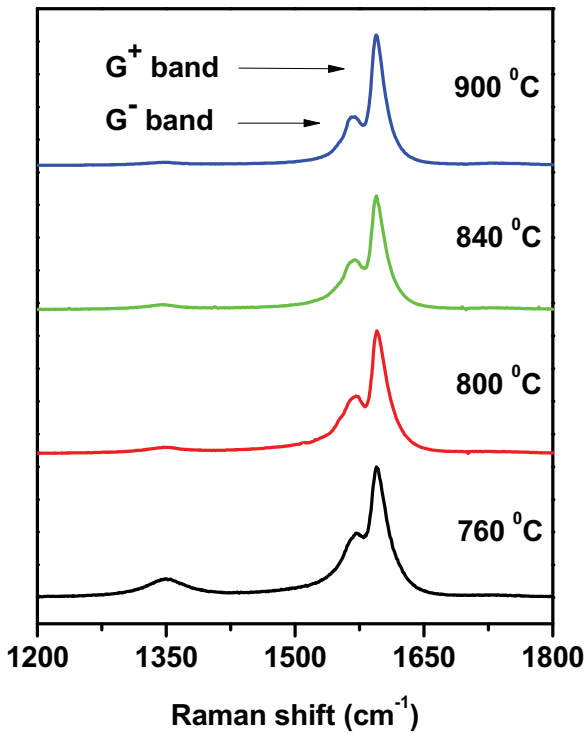

Figure 5.9: G^- and G^+ bands of the samples prepared by Triethyl borate at several temperature.

carried a detailed study of this peak position for different growing temperatures and for tubes prepared using Triethyl borate, Triisopropyl borate and Ethanol. This study is summarized if Fig 5.12, that shows an upshifted peak for both boron containing samples. The error bars on this figure are due to an average on the spectra obtained from different spots on the sample.

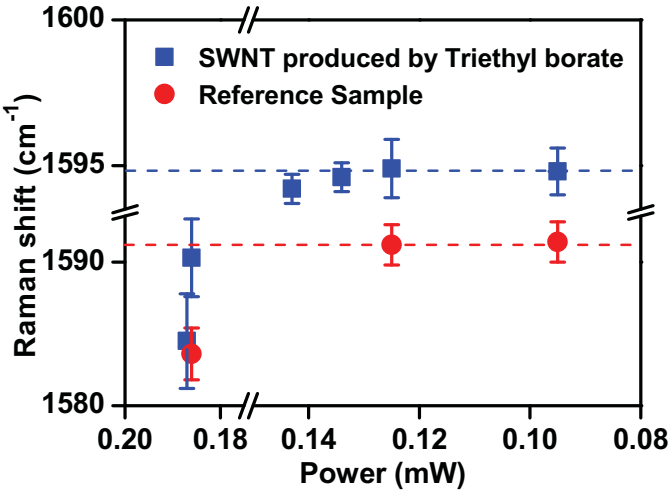

Figure 5.10: G^+ band of a sample prepared by Triethyl borate, a reference sample and the laser power. As expected (11), it is clear that a higher laser power heats the sample softening the G band position, that remains constant for a power bellow $\sim$ 0.13 mW. The dash line is just to guide the eye. The error bars are due to different points on the sample.

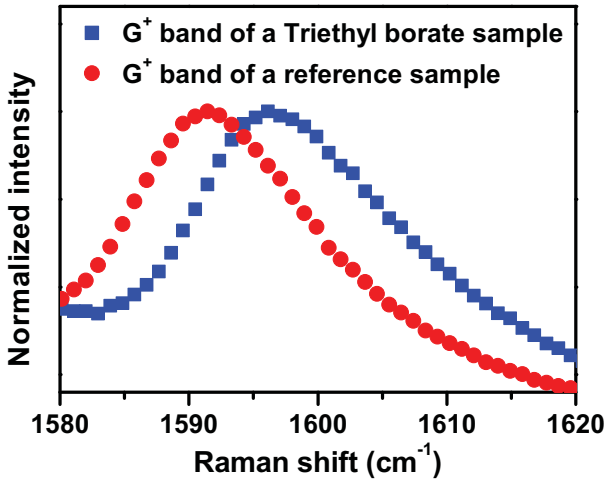

Figure 5.11: Typical G^+ band upshift on the sample prepared by Triethyl borate using a laser power around 0.13mW. An upshift of $\sim$4cm^{-1} is observed.

This upshift can not be explained by a heating process, and is an evidence for boron on the carbon SWNT structure, since the lowering of the Fermi level is expected to shift the position of the G band to a higher value (40, 48, 51). However, it is still possible that this shift is caused by charge transfer of some of the impurities, such as B_2O_3, there are present on the sample, as we will see

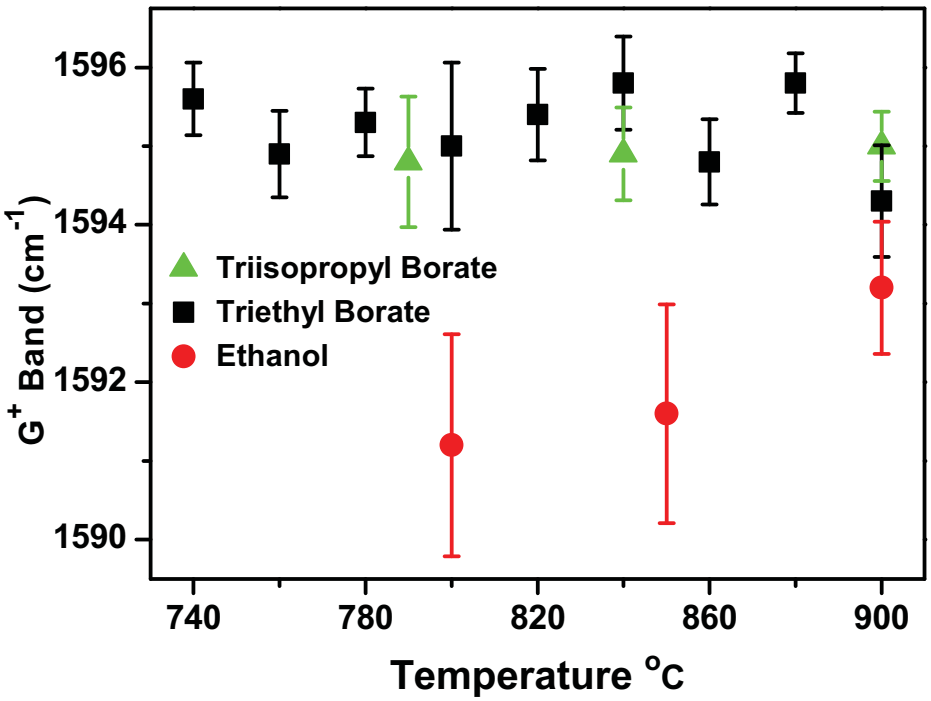

Figure 5.12: G^+ band position for different growing temperatures and precursors. Laser power used was around 0.13mW. The error bars are due to different points on the sample.

on the XPS section. But as we will see on that section, the concentration of impurities like those are not constant at samples produced at different production temperatures, indicating that this shift maybe not caused by them.

Such feature was not observed with this large intensity for tubes prepared by other techniques such as laser ablation with boron incorporated on the carbon target (36, 52). We believe that there is at least two reasons for the lack of observation of this upshift for those tubes. The first one is that laser ablation may produce tubes similarly to the arc discharge technique, producing BC_3 nanodomains instead of truly doping the tubes in the sense of substitute a carbon atom by a boron one. And as described on the preceding chapter, for the BC_3 nano island case, the Fermi level is not so shifted as in the case of substitutional doping (10). Another possibility is that even though such technique produces a substitutional doping, only a very low boron concentration is incorporated on the tubes, even if they are prepared using a high concentration of boron to carbon on the targets (36). On both cases, a higher amount of boron on the targets would be necessary to shift the G band of those tubes to a similar position that we observed for our samples. However,

amounts higher than 3% of boron on the targets leads to no tubes formation (36), thus making a higher upshift of the G band impossible to be probed in such production methods. In order to make the above statements more clear, we must prove that our tubes have a higher boron concentration than the tubes produced by laser ablation. This proof will be given on the next section, where XPS data will be analysed.

The G band of the Raman spectra of our tubes provided one evidence that our tubes are doped with boron, and that this doping level is higher in comparison to the tubes produced with laser ablation.

5.4.4
Raman spectra: The G′ band

The G′ band is due to an allowed second order phonon process presented on all sp^2 carbon structures (11, 44). This band is located between 2500^{-1} to $2800cm^{-1}$, is sensitive to the laser energy, tube's diameter and is very useful on the characterization of sp^2 materials (11, 44).

Raman measurements performed on carbon nanotubes related changes on this band with the doping on the structure (53). It was found that a n type doping creates a defect induced G′ band at lower frequency besides the pristine G′ band that has the position unaltered during the Raman measurements on different parts of the tube. The same induced G′ band appear for a p type doping, but on the right side of the pristine G′ band.

It is important to notice that despite been observed on some Raman measurements, such induced peak has never been observed on other Raman measurements of supposed boron doped tubes. Actually, it was already observed a downshift of the peak instead of an upshift (54, 39), even on the samples that were synthesized on the same way as the sample analysed by the Raman measurements that observed the upshift (36, 37).

As shown in Fig 5.13, we were not able to differentiate between this band from the reference SWNT sample to a sample prepared by Triethyl borate. More than that, the peaks that we found are well fitted by the equation for position of the defective and pristine G′ band of carbon SWNTs (12), showing that our peaks are mainly related to the low doping environment of the tubes.

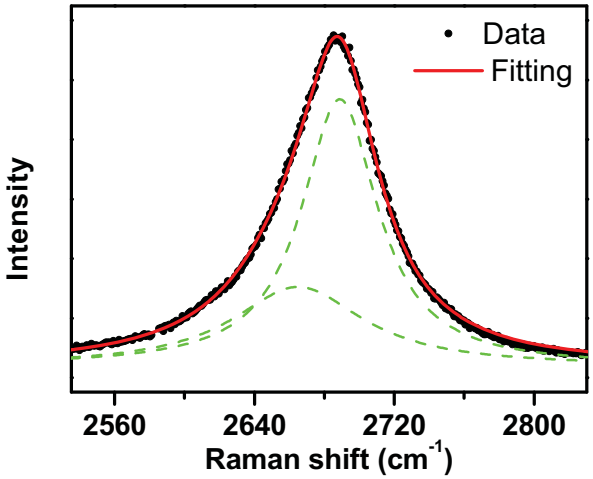

Figure 5.13: Typical G′ band position of a sample prepared by Triethyl borate. It is possible to fit the spectra by the positions provided by the equation of (12). The laser power used was around 0.13mW.

The analysis of the G′ band could not provide any further information regarding the doping level of our samples.

Raman characterization provided us with useful informations about our samples. Now we know that we produced single wall carbon nanotubes, and in accordance with the TEM images, the diameters are around 1nm with increasing diameters among highest production temperatures. We also know that tubes produced with both boron containing precursors have a lower D band in comparison to tubes produced by Ethanol, meaning that those tubes may have less defects on the structure. The G band of the tubes prepared by both boron containing feedstock showed an upshift in comparison to pure carbon SWNTs. Since all measurements were carefully made, using the same parameters, this shift can be considered as an evidence for the lowering of the Fermi level, thus indicating that those tubes may be doped with boron.

5.5 X-ray Photoelectron Spectroscopy - XPS

Each element on the periodic table have electrons bonded to the charged nucleus. Resulting from the Schrodinger equation, the energy level of those electrons are determined by the number of protons on the nucleus and by the electron-electron interactions, in other words, each element is well defined by the binding energy of the electronic structure. When the atoms are combined into molecules or in a larger structure, this energy changes a little, but still

can be related to the elements and to the the chemical bond that they are performing (55).

Briefly speaking, the XPS technique is capable of measuring those changes on the binding energy of the electrons of the sample that is being tested. To do this, a X-ray beam is focused over the sample, making some electrons to be ejected from it. The kinetic energy of those electrons is then measured, and since the energy of the incident photon is known, a simple calculation can lead us to the binding energy that the measured electron had on the sample (56, 57).

A variety of other phenomena can happen during the XPS measurement. As an example, the Auger effect happens when the leaving electron leads a vacancy on the material, and then, an electronic transition of a higher energy electron occur into this empty energy level. The resulting energy of this transition leads to a emission of an Auger electron. This electron is then measured by the XPS' detector, creating a well positioned energy peak on the resulting energy plot. The main difference of this peak to the peaks described on the above paragraph, is that the energy of the Auger electron is independent of the X-ray energy, since this last energy is high enough to ionize the first emitted electron. In this way, the kinetic energy of the Auger electron does not change with the choice of the X-ray source (56, 57).

Our measurements were performed with a Magnesium K_α X-Ray line and a VG Thermo Alpha 110 hemispherical analyser. We could use an Aluminium K_α X-ray source, but for our case, we avoid it's use because it produces an Auger peak near the 1s carbon peak. And this line also results in a lower energy resolution in comparison to the Magnesium line. To fit the resulting energy plot we used a Voigt line shape, that is a convolution of a Lorentzian and a Gaussian curve. This combination rises due to the Lorentzian XPS cross section and to the Gaussian analyser. We also used a Shirley curve to fit the background, which is a standard procedure for this kind of analysis (56, 57).

All of our samples were carried to the XPS analyser. A survey spectrum with 0.5eV of energy step were done for energies ranging from 0eV to 1100eV and a local energy spectrum with 0.1eV of energy step were done for carbon and boron energy positions. Fig 5.14 shows a typical survey spectrum of a sample prepared using Triethyl borate at 800^0C.

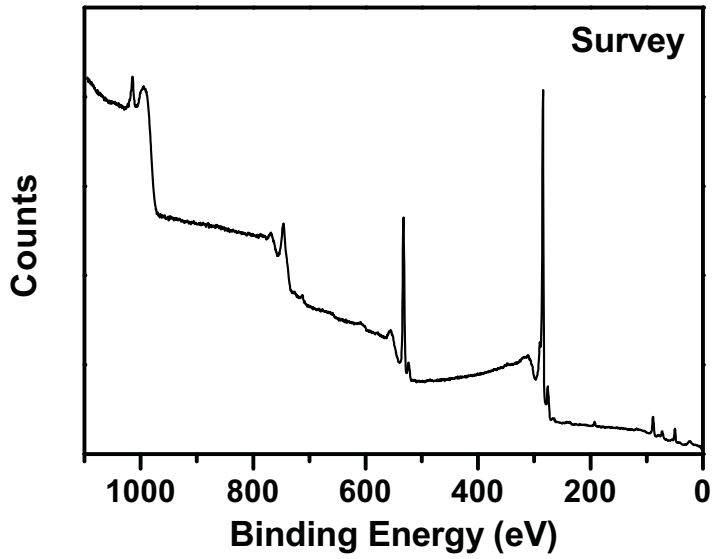

Figure 5.14: Survey XPS spectrum of a sample prepared using Triethyl borate at 800^0C.

As expected we found a carbon 1s core peak at 284.5eV for our samples (58, 33). The lack of observation of a small shoulder at 281.8eV that is related to the presence of boron and carbon systems such as B_4C (33) can be due to limitations of our XPS or to a low doping concentration of our samples. Fig 5.15 shows two of those carbon 1s peaks for two different growing temperatures. The other temperatures have similar XPS peaks.

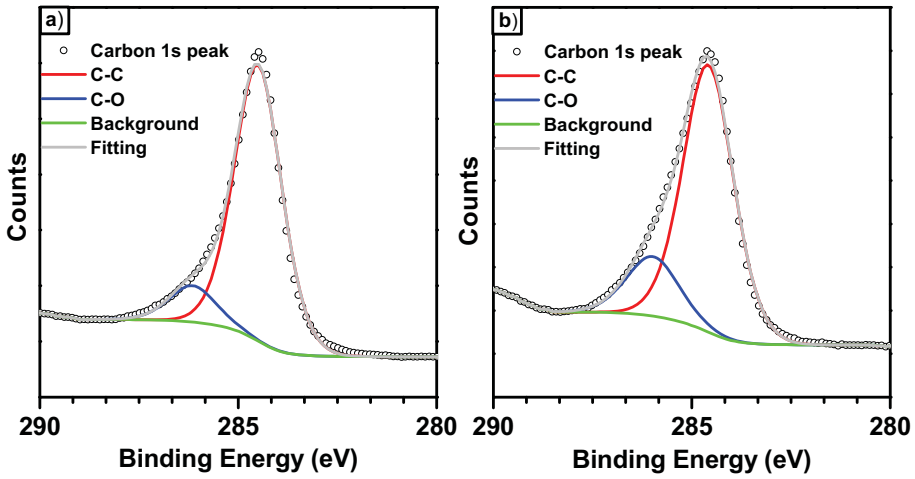

Figure 5.15: XPS of carbon 1s peak for the samples prepared at a) 800^0C and b) 860^0C.

XPS analysis of the boron peak on the samples shows the presence of multiples boron compounds, as shown in Fig 5.16, where we present two XPS spectra taken from samples prepared at 800°C and 860°C. The peak at 193.1eV can be attributed to B_2O_3 (58), and the peak at 192.4eV can be due to the formation of a boron and magnesium compound such as $Mg_3B_2O_6$ (59). We also have found a peak around 189.8eV that can be related to Boron oxide states or it is due to the formation of BC_2O (58). It was also possible to find small traces of B_4C around 187.5eV (58) on samples prepared at temperatures higher than 880°C. The spectra obtained from all samples prepared by Triethyl borate at different temperatures are quite similar to the spectra presented on Fig 5.16, but as pointed on the G band section, with different impurities concentration.

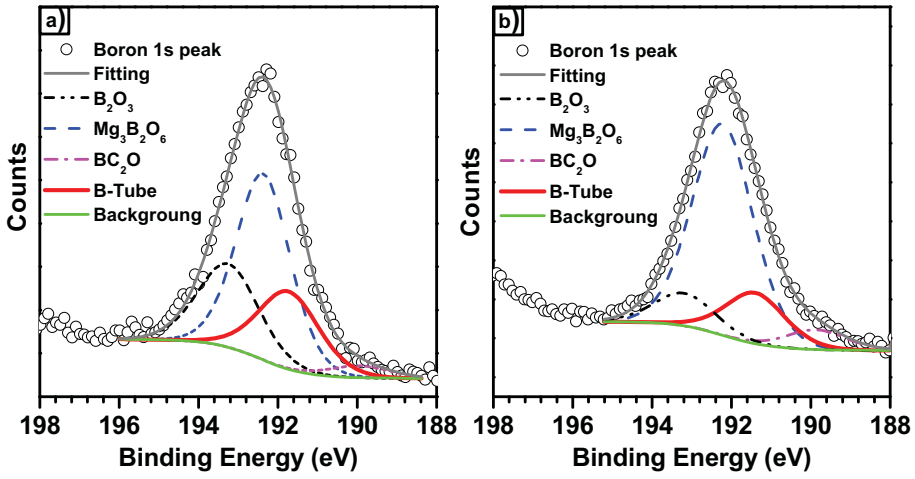

Figure 5.16: XPS of boron 1s peak for the samples prepared at a) 800^0C and b) 860^0C.

As shown in Fig 5.16, we found a peak from 191.4eV to 191.8eV in all boron containing samples. The elemental boron 1s peak is at 188eV (58) and the peak for boron doped graphite is at 188.5eV (58). There are some experimental evidences, but with no theoretical calculations, showing that the cylindrical structure of the SWNT makes this energy to be around 191.4eV to 192.1eV (33, 37, 60). This shift on the binding energy would be caused by the increase of the sp^3 hybridization caused by the SWNT structure and would be diameter dependent, thus a SWNT with a larger diameter would have a smaller shift when compared to a thinner SWNT.

In order to confirm or refute this peak position, professors Rodrigo B. Capaz and L.A. Terrazos, made DFT calculations on a (10,0) doped SWNT and on a doped graphene sheet. They found a binding energy for the 1s orbital

of the boron atom that is ∼2.9eV lower when this element is substitutionally positioned in the SWNT structure than in a graphene sheet. This correspond in a ∼2.9eV upshift of the boron 1s core level on the XPS analysis. In this way, the boron 1s peak on the XPS analysis of a (10,0) SWNT is located at ∼191.4eV. This result shows a great correspondence between theory and experiment, even considering that the diameter of a (10,0) SWNT is 0.8nm, that is on the lower end of our diameter distribution. This small discrepancy may be explained by experimental and theoretical imprecisions, some chirallity influence rather than only diameter influence and by the fact that our RBM analysis is not able to fully provide the diameter distribution of the samples. In my opinion it is important to note that a (n,n) tube bends all chemical bonds of the doped boron atom while a (m,0) tube with similar diameter only bends two chemical bonds. In this way, I expect that the (n,n) SWNT will have an enhanced upshift of the boron 1s peak in comparison to a (m,0) tube with similar radius.

Identifying those peaks between 191.4eV to 191.8eV with the substitutional boron on the SWNTs, and by comparing the areas of the carbon and boron fitted curves and taking in account the respective sensitive XPS factors, we found a doping level around 1.2±0.3at% for all the samples produced by Triethyl borate and 0.8±0.3at% for the samples produced by Triisopropyl borate.

One interesting point to note is that the total boron to the total carbon concentration on the samples is very small when compared with the initial stoichiometry of those elements on Triethyl Borate. This can be explained by the formation of a white film characteristic of boron oxides and boric acid on the quartz tube, on the entrance of the furnace, since those substances are soluble in water, that was used to clean the tubes before each growth. And that is main reason for the concern presented on the first section of this chapter.

We also used XPS to develop a simple method to determine the temperature range that optimizes the boron doped SWNT production. It is reasonable to consider that magnesium will not leave the sample in a some volatile species. We can also suppose that the majority of C-C bonds will be on the SWNTs, and since we have used the same catalyst on the different production temperatures, the plot Carbon at%/(Carbon at% + Mg at%), where we denote by Carbon the area of the peak at 284.5eV, may be a good indication of the most efficient temperatures regarding the production of the tubes. This ratio is plotted in Fig 5.17. This plot is in accordance with the amount of tubes observed at the FEG SEM images at different production temperatures. In fact, there is a plateau in the temperature range from 760°C to 840°C that

are the same in which we observed the greater concentration of tubes on the FEG SEM images. The lower values of this plot corresponds to the images with less amount of tubes, confirming our initial guess regarding the majority of C-C bonds on the SWNTs, and indicating that this plot can be very useful in determining quantitatively the temperature range with the highest yield of produced tubes in a HVCVD system, since a solid phase element from catalyst is present in the sample throughout the process. With this in mind we can estimate that the sample prepared at 800°C has ∼2 times more tubes than any other temperature that we measured on the XPS. And it has ∼7 times more tubes than 860°C and ∼15 times more tubes than 900°C.

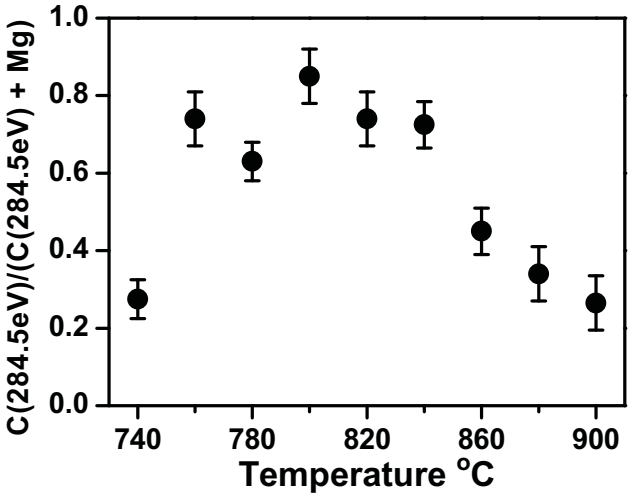

Figure 5.17: Plot of Carbon at%/(Carbon at% + Mg at%) for each growing temperature.

As expected by the discussion made on the Raman spectroscopy section, the doping values found by XPS are above the values found for tubes prepared by the laser ablation technique, which is less than 0.3%, even for the targets with a high boron concentration (36, 37). This results shows the consistency of the measurements and interpretations made so far on the Raman spectroscopy and XPS technique.

5.6 Agreement between XPS and Raman characterization

In order to make the last paragraph more clear and to show the consistency between the Raman and XPS characterization, we applied a simple formula that was used on the study of electron acceptors on graphite intercalation compounds (GICs) (51) on the G^+ bands of our samples. This equation relates the shift of the G band $\Delta\omega$, and the charge transfer Δf, for high charge

transfer of the electron acceptor per carbon atom of the structure in a simple way $460\Delta f \sim \Delta\omega$. Under the assumption that the substitutional boron doping is introducing a hole into the structure of the SWNT (16), and that the charge transfer is big enough for us to use this equation, we expect to obtain a good agreement between the doping levels found by XPS and by this formula, due to the similarities between graphite and carbon nanotubes.

The main reason to not use this rule or any other rule on the Raman results before any XPS analysis, is because despite several studies pointing out that exist a correspondence between $\Delta\omega$ and the doping level, they were carried by applying a gate voltage on the tubes in order to shift the Fermi level and looking for changes on Raman spectra, (40, 48) but they didn't compare their results with doped tubes and didn't provide any easy rule to make a doping level estimative. So, at that time, there was no easy way to relate the Raman shift to the substitutional boron doping concentration on SWNTs, and any attempt to use some formula would be worthless without the XPS data. We expect not just to obtain a good doping estimative using the formula obtained for GICs, but to improve it for boron doped SWNTs.

The plot of Fig 5.18 shows that the doping concentration obtained through the relation used for electron acceptors on GICs $460\Delta f \sim \Delta\omega$ is a good estimative to the doping levels found on the XPS measurements for both boron precursors, showing that the G^+ band upshift is probably related with the charge transfer between the boron atoms and the structure of the carbon nanotube. It is important to note that we used the sample produced by Ethanol at 850^0 as an undoped reference sample.

It is clear that despite being used on the study of GICs, the relation $460\Delta f \sim \Delta\omega$ works pretty well for boron doped tubes with a doping level around 0.8% to 1.5%. However, since a SWNT is not a GIC, we improved this formula to best fit our XPS results, and in order to rewrite this equation for SWNTs, we used all of our data to obtain a better parameter k for a new formula $k\Delta f \sim \Delta\omega$. With this fitting we got a new relation that estimates our data with a better precision. The obtained k is around $420 \pm 50 \mathrm{cm}^{-1}\mathrm{charge}^{-1}$, which is still in accordance with the previous value, and Fig 5.19, that is very similar to Fig 5.18, shows a plot using $k = 420\mathrm{cm}^{-1}\mathrm{charge}^{-1}$. It is possible to observe that this relation gives a good estimative for SWNTs with a doping concentration on the range of 0.8% to 1.5%.

More important than Fig 5.19, is the comparison between this obtained formula with other results found on the literature. However, there is a lack of reported upshift on boron doped SWNTs. In order to overcome this problem, we also used the reported data found for boron doped double wall carbon

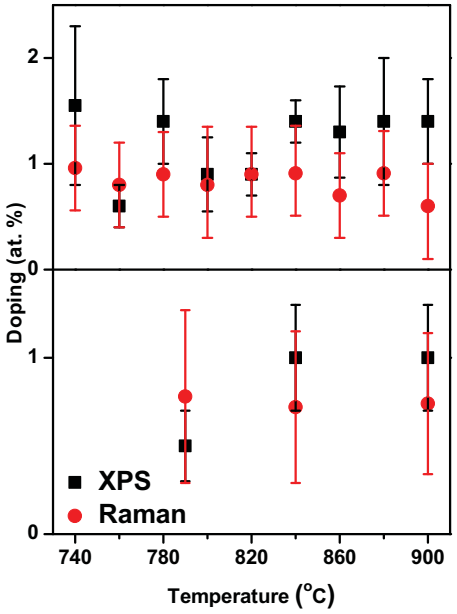

Figure 5.18: Doping comparison between XPS measurements and the predicted value obtained using the formula $460\Delta f \sim \Delta\omega$. The upper graph is the measurements done for the samples prepared using Triethyl borate and the lower graph shows the measurements for the samples synthesized using Triisopropyl borate.

nanotubes prepared by CVD (60, 54). XPS and EELS measurements shows that those tubes have a doping level ranging from 0.4% to 1.4%, which is higher than the doping concentration found on SWNTS produced by laser ablation technique (36, 37). This higher doping level causes a detectable change on the position of the G band on the Raman spectra of those tubes. Table 5.3 shows the comparison between the doping level found by XPS and by the obtained formula $(420 \pm 50)\Delta f \sim \Delta\omega$ for those works.

Table 5.2: Comparison between XPS and $420\Delta f \sim \Delta\omega$ for boron doped DWNTs (60, 54) and SWNTs (39) with increasing boron concentration.

XPS measurement (at. %)	$\Delta\omega/(420 \pm 50)$ **(at. %)**	**Reference**
0.4	0.5±0.1	(54)
0.8	0.7±0.1	(54)
1	1.0±0.1	(60, 39)
1.4	1.2±0.2	(54)

The results above show that the obtained formula is in agreement

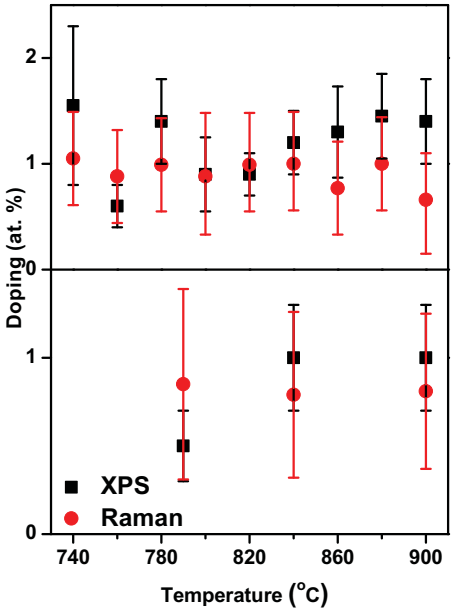

Figure 5.19: This plot shows the fitting using the new parameter $k \sim 420$ obtained from the experimental data. The upper graph is the measurements done for the samples prepared using Triethyl borate and the lower graph shows the measurements for the samples synthesized using Triisopropyl borate.

with other techniques, such XPS, since it is capable of performing a good doping level estimative for the substitutional boron doping concentration on single and double wall carbon nanotubes, and enhances the evidence that the observed shift is caused by the doping, rather than anything else. This equation has the advantage of providing a fast and easy way to estimate the doping concentration in the high doping regime, since Raman spectroscopy can be applied on most kind of samples, even on individual tubes, that is of fundamental importance on the characterization of this material on nanodevices.